 doi:10.20944/preprints202112.0044.v1

Article

Linear Quadratic Regulator and Fuzzy Control for Grid-Connected Photovoltaic Systems

Azamat Mukhatov [1], Nguyen Gia Minh Thao [2] and Ton Duc Do [1,*]

[1] Department of Robotics and Mechatronics, School of Engineering and Digital Sciences Nazarbayev University, Nur-Sultan, Kazakhstan; azamat.mukhatov@nu.edu.kz
[2] Graduate School of Engineering, Toyota Technological Institute, Nagoya city, Japan; nguyen.thao@toyota-ti.ac.jp
* doduc.ton@nu.edu.kz

Abstract: This work presents a control scheme to control the grid-connected single-phase photovoltaic (PV) system. The considered system has four 250W solar panels, a non-inverting buck-boost DC-DC converter, and DC-AC inverter with LCL filter. The control system aims to track and operate at the maximum power point (MPP) of PV panels, regulate the voltage of DC link, and supply the grid with a unity power factor. To well achieve these goals, the proposed control system consists of three parts, that are MPP tracking controller module with a fuzzy-based modified incremental conductance (INC) algorithm, a DC-link voltage regulator with a hybrid fuzzy proportional-integral (PI) controller, and a Current Controller module using the linear quadratic regulator (LQR) for grid-connected power. Based on fuzzy control and LQR, this work introduces a full control solution for grid-connected single-phase PV systems. The key novelty of this research is to analyze and prove that the newly proposed method is more successful in numerous aspects by comparing and evaluating the previous and present control methods. The designed control system settles quickly, which is critical for output stability. In addition, as compared to backstepping approach used in our past study, the LQR technique is more resistant to sudden changes and disturbances. Furthermore, backstepping method produces the larger overshoot, which has a detrimental impact on efficiency. Simulation findings under various weather conditions were compared to theoretical ones to indicate that the system can deal with variations in weather parameters.

Keywords: fuzzy control; grid-connected; incremental conductance algorithm; linear quadratic regulator; maximum power point tracking; photovoltaic system

1. Introduction

Renewably energy is emerging as one of the main sources of energy for the future. The key reason for this is the depletion and pollution of fossil fuels. On the other hand, the renewable energy sources are available, clean, eco-friendly, and cost-effective. There are various types of renewable energy sources, in which solar and wind energy systems have become more and more popular in many countries. According to [1] and [2], harmonic resonances, that often occur in grid-connected wind power farms, cause negative effects to the power quality of the grid.

Nowadays, the solar energy has been widely used around the world and demonstrates impressive results. To effectively obtain electricity from solar energy, photovoltaic (PV) systems should be installed. The system efficiency is strongly affected by two major factors as follows [3, 4],

a) Weather factors such as the air temperature and solar radiation
b) Hardware factors such as power electronic devices and system loads.

While the prior factor is uncontrollable, the second one depends on the designer, system operator and electric grid. To improve the efficiency of the power electronic parts,

Preprints (www.preprints.org) | NOT PEER-REVIEWED | Posted: 3 December 2021 doi:10.20944/preprints202112.0044.v1

appropriate converter topologies together with efficient control schemes are required. From [5–8], there are two modes of operation for the PV systems that are,

- Stand-alone mode
- Grid-connected mode

Between these two modes of operation, the grid-connected mode is preferable as it can avoid the issues of storage systems in the stand-alone mode. For grid-connected systems, the following two problems need to be solved simultaneously [7–9]:

- Management of several combined systems
- Regulation of each power stage or system.

For the second problem, it often requires the following tasks: 1) Tracking the maximum power point (MPP); 2) Minimizing the harmonics, which usually make negative effects to the power grid and devices; 3) Maintaining the DC-link voltage within a desired range; 4) Keeping the unity power factor at the output of the filter [10].

One of the most important parts of this research is the MPP tracking part, which is mainly used to find and keep the output power of a PV panel at its maximum value [11]. The MPP tracking (MPPT) technique can be divided into two main categories: the perturb and observe (P&O) technique and incremental conductance (INC) algorithm. The principle of the INC technique is simple, the system calculates for dI/dV, where I is the current and V is the voltage of the circuit and adds both the parts; so if the result of I/V+dI/dV is zero, it means that the system has already reached the MPP; if the result is less or more than zero, the system should increase or decrease the duty ratio of the associated DC-DC converter, respectively. This is a closed-loop, maintaining the MPPT despite of the fast-varying conditions [12]. The negative side of this algorithm is its high computational complexity, but on the contrary, it leads to high efficiency. In case of the P&O technique, it measures voltage and current values to estimate the power of the solar panel periodically and compares it with the previous one. If the power of the PV module is increased (dP/dV>0), the system will start adjustment in that direction, otherwise in the opposite way. These operations will continue until system finds MPP. In fact, the technique depends on the perturbation of the voltage, so if the perturbations are high, speed of the technique is fast. The advantages of this method are simplicity without interests in the previous PV characteristics, however the main drawback is oscillations happening near the MPP which may lead to power losses in varying-weather conditions [10]. The INC type is more advantageous in terms of accuracy in finding and tracking the MPP, compared to the second type; therefore, in this paper, the INC algorithm is improved by the fuzzy control and then implemented in the grid-connected PV system.

Considering current controller strategies, generally, they can be divided into two main parts: on/off controllers and pulse width modulation (PWM) based control techniques [13]. The first group has two subdivisions which are hysteresis control and predictive control. Hysteresis control has high dynamics and fast response; however, its major drawback is variations of the switching frequency and high complexity of the system. Predictive control has positive sides such as less computation time, better regulation, and decrease in offset error. On the other hand, it is required to identify proper model for the system and the installation cost of the system is high. The second group can be divided into as linear and non-linear control [13]. Proportional-integral (PI) is the well-known classical control technique, which can be easily designed for controlling the current. However, the key disadvantage of this controller is its poor compensation of lower-order harmonics and presence of steady-state errors [14]. The proportional resonant (PR) can compensate for the harmonics. Moreover, this type of controller has high dynamics, less complex and can reach a high gain at the resonance frequency. However, this controller has a problem with reaching the power factor control, which means that the system is not able to control the losses in the system [15].

Generally, the power factor is a ratio between working power and apparent power. Thus, if there is no control/maintenance of high-power factor, consequently the system efficiency is low. On the other hand, the predictive deadbeat control has high level of har-

 doi:10.20944/preprints202112.0044.v1

monic compensation and rapid fast-tracking performance. The disadvantage of this controller is that it requires a lot of computation efforts [16]. The harmonic compensation and steady-state error can also be done by repetitive controllers; but its slow tracking response is the main drawback [17]. Fuzzy logic controller (FLC) [13] is one of the popular intelligent control techniques. This is extensively used in the renewable energy systems due to its efficiency and easiness in usage. It is also robust and applicable to a wide range of the dynamics systems from linear and nonlinear systems. Moreover, this type of controller can perform complex estimations which is not possible to do with conventional methods [11]. Linear quadratic regulator (LQR) is an effective control method which is applicable for both linear and nonlinear systems. In this method, the control gain is designed to minimize a quadratic cost function, by selection of appropriate weighting matrices. In our study case, the cost function is the quadratic function of the tracking error between current and its reference and the control efforts. This technique was chosen to be implemented due to its properties such as stability, robustness, and ease in application. Moreover, the computational complexity of the LQR controller is not high, which means that it is fairly simple to implement.

This paper proposes a complete control solution for grid-connected single-phase PV systems based on fuzzy control and LQR. Our past related research on this topic was conducted with a different type of controller, namely backstepping method [18]. The present study is a significant extension and improvement of our former research in terms of enhancing the quality of control method. The proposed technique is the LQR in appropriate combination with fuzzy control and improved INC algorithm for grid-connected photovoltaic systems; furthermore, detailed explanations on developing the fuzzy association rules of the designed fuzzy logic controllers are newly presented in this study. The main originality of this paper is to show and prove by comparison of our former and present control methods that the newly suggested method is more effective in various aspects. Specific details of the PV system and controllers can be found in our past work in [18], which was used as the basis for this paper. The major advantage of the LQR method is its ability to react in rapid manner to the changes of the system, namely, changes in the air temperature or solar irradiation. In other words, the system can reach its settling time faster, which is important to stabilize the behavior of output. Moreover, it can be said that LQR technique is robust to different disturbances and changes compared to backstepping technique. In addition, backstepping method has the higher overshoot which significantly impacts the efficiency in a negative way. As it was mentioned above, the speed of the LQR is faster, which makes such kind of controller more preferable. These are the key contributions of this study compared to that of our past research in [18]. Simulation results under different weather conditions show that the proposed control system can cope with changes in weather parameters effectively and were compared with theoretical ones. Moreover, it was shown that the variations in weather parameters do not much affect the performance of the proposed control system.

The remains of the paper are organized as follows. Section II shows the modeling of the grid-connected PV system, that includes the system description, PV panel model, and modeling of power converters. The control system design is shown in Section 3, which consists of the MPPT control module, DC-link voltage regulator module, and current controller module. In addition, Section IV provides simulation results in MATLAB, in which the first test case is with a fixed ambient temperature, and the second test case is with an unchanged solar irradiation. The comparison and assessment of efficacy between the LQR control method in this study and backstepping approach in our past work [18] are presented in Section 5. The conclusions are described in the last section.

2. PV Grid-Connected System Modeling

2.1. System description

This paper considers a grid-connected PV system consisting of two stages of power conversion. The nominal power of the system is 1 kW. Figure 1 shows the circuitry of the

Preprints (www.preprints.org) | NOT PEER-REVIEWED | Posted: 3 December 2021 doi:10.20944/preprints202112.0044.v1

system: the power generated from PV array is directed to the non-inverting buck-boost DC-DC converter. After that, to supply the grid, the obtained result is converter to AC via single phase DC-AC inverter. To get rid of unwanted noises and disturbances injected to the grid, the LCL filter was used [19, 20].

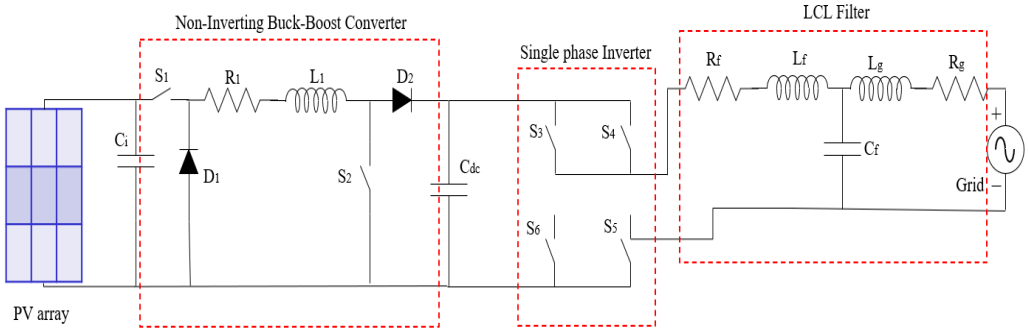

Figure 1. PV single-phase grid-connected system

2.2. PV Panel Model

The PV panels used in this paper have characteristics as presented in [18]. The provided data is applicable when the temperature is 25 °C and the solar radiation is 1000 W/m². In total, the PV array consists of four panels, where the nominal power of each panel is 250 W. Figure 2 shows the impacts of temperature and solar radiation to the power and voltage, respectively. Table 1 represents MPPs of the PV panel and array in terms of power and voltage.

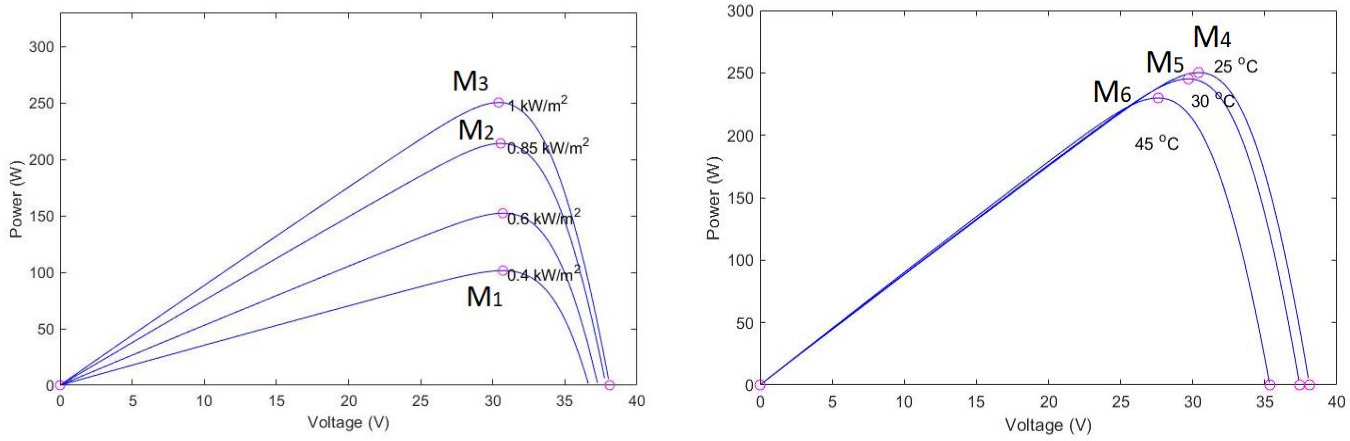

(**a**) (**b**)

Figure 2. Power obtained from PV panel for different (**a**) solar radiation values and (**b**) temperature values.

Table 1. Power and Voltage at Maximum Power Points.

MPPs	M1	M2	M3/M4	M5	M6
V_P (V)	29.3	30.32	30.4	29.8	28.04
$P_{P,panel}$ (W)	95.9	211.7	250	244.8	225.7
$P_{P,array}$ (W)	383.6	846.8	1000	979.2	912.8

2.3. Modeling of Converters

Figure 1 particularly illustrates all components of the system including the single-phase inverter and non-inverting buck-boost converter [7]. Input control signals of the non-inverting buck-boost converter and single-phase inverter are α_P and β_P, respectively.

Preprints (www.preprints.org) | NOT PEER-REVIEWED | Posted: 3 December 2021 doi:10.20944/preprints202112.0044.v1

$$\alpha_P = \begin{cases} 0 \text{ ; } S_1 \text{ and } S_2 \text{ are OFF} \\ 1 \text{ ; } S_1 \text{ and } S_2 \text{ are ON} \end{cases}$$

$$\beta_P = \begin{cases} 1 \text{ ; } S_3 \text{ and } S_5 \text{ are ON, } S_4 \text{ and } S_6 \text{ are OFF} \\ 0 \text{ ; } S_3, S_4, S_5 \text{ and } S_6 \text{ are OFF} \\ -1 \text{ ; } S_3 \text{ and } S_5 \text{ are OFF, } S_4 \text{ and } S_6 \text{ are ON} \end{cases}$$

The modeling technique, specifically averaging, and Kirchhoff's laws were used to estimate a mathematical model for the two converters. Equation (1) and Table 2 demonstrate details of the previously mentioned procedure

$$\begin{cases} \dot{x}_1 = \frac{1}{C_i}\bar{I}_P - \alpha\frac{1}{C_i}x_2 \\ \dot{x}_2 = \alpha\frac{1}{L_1}x_1 - \frac{R_1}{L_1}x_2 + (\alpha-1)\frac{1}{L_1}x_3 \\ \dot{x}_3 = (1-\alpha)\frac{1}{C_{DC}}x_2 - \beta\frac{1}{C_{DC}}x_4 \\ \dot{x}_4 = \beta\frac{1}{L_f}x_3 - \frac{R_f}{L_f}x_4 - \frac{1}{L_f}x_5 \\ \dot{x}_5 = \frac{1}{C_f}x_4 - \frac{1}{C_f}x_6 \\ \dot{x}_6 = \frac{1}{L_g}x_5 - \frac{R_g}{L_g}x_6 - \frac{1}{L_g}V_g \end{cases} \quad (1)$$

Table 2. Variables

Variable	Symbol in Figure 1	Averaged variable in (1)
PV array voltage	V_P	x1
Current through the inductor L_1	i_{L1}	x2
DC link voltage	V_{DC}	x3
Input current of the LCL filter	i_f	x4
Voltage on the capacitor C_f	V_{Cf}	x5
RMS value of the electric grid current	i_g	x6
Control signal of the non-inverting buck-boost DC-DC converter	α_P {0, 1}	α (0, 1)
Control signal of the single-phase DC-AC inverter	β_P {-1, 0, 1}	β [-1, 1]
PV array current	I_P	$\bar{I}_P$
RMS value of the electric grid voltage	V_g	V_g

3. Control System Design

The design of the control system considered in this study is shown in Figure 3 and includes three main parts, such as the MPPT controller, DC link voltage regulator, and current controller. In this paper, the detailed explanations on developing the fuzzy rules of the two designed fuzzy logic controllers are newly presented, which are useful in reference to design other fuzzy controllers.

Preprints (www.preprints.org) | NOT PEER-REVIEWED | Posted: 3 December 2021 doi:10.20944/preprints202112.0044.v1

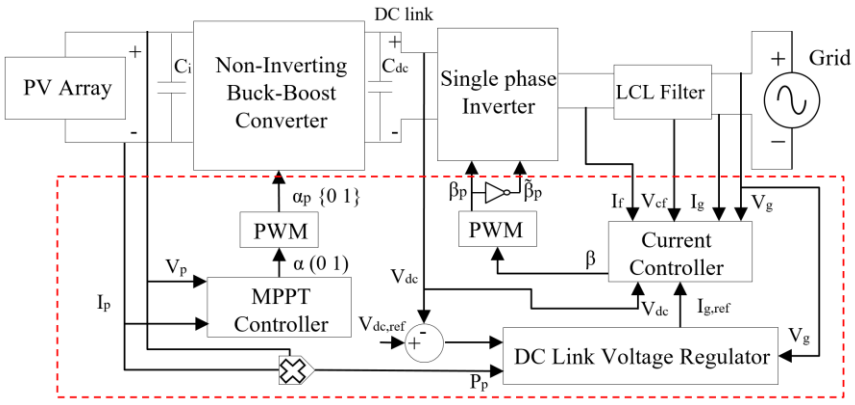

Figure 3. System schematics in detail.

3.1. The MPPT controller module

The PV array produce its optimal power despite the varying weather with a help of the designed MPPT controller. According to Figure 4, this controller consists of two parts, that are fuzzy logic controller (FLC-1) and first Proportional-Integral (PI-1) controller.

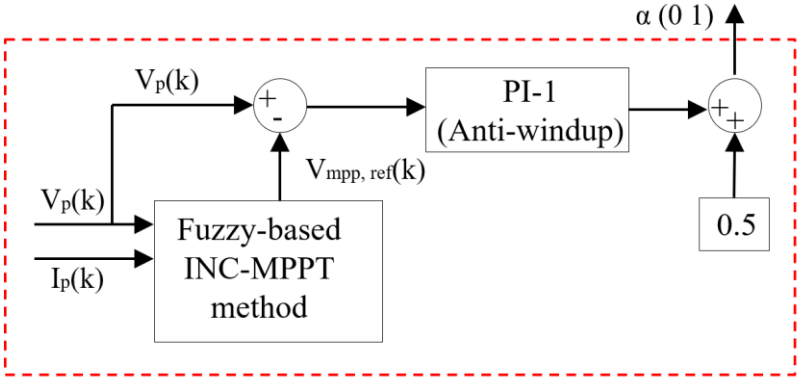

Figure 4. MPPT controller module schematics

3.1.1. FLC-1

The main idea of this sub-controller is to improve the conventional INC-MPPT algorithm in terms of response time and efficiency by combining it with fuzzy logic controller (FLC-1). According to Figure 5, the FLC-1 has two inputs and one output. The first input can be two kinds:

- $|A_P(k)|$ - the absolute value of a modified slope of power-voltage (P-V) curve as expressed in (2). This equation also includes a pre-scaling module $G_P(k)$ as shown in (3).
- $|dI_P(k)|$ - the change in the current of PV panels in absolute value.

$$A_P(k) = G_P(k)[S_P(k)] = G_P(k)\left[I_p(k) + V_p(k)\frac{dI_P(k)}{dV_P(k)}\right] \quad (2)$$

$$G_P(k) = \frac{1}{1 + g_1\left[\frac{P_P(k)}{P_{P,total}^{max}}\right]} \quad (3)$$

where $P_{P,total}^{max}$= 1000 W is the maximum power of PV panels, g_1 is a positive coefficient. The second input is the INC algorithm's prior step-size ΔV(k-1). Figure 6 shows the detailed flowchart of the proposed methods. In addition, the aforementioned scaling module $G_P(k)$ is used to suitably increase the sensitivity of slope $S_P(k)$ as illustrated in Figure 7.

Preprints (www.preprints.org) | NOT PEER-REVIEWED | Posted: 3 December 2021 doi:10.20944/preprints202112.0044.v1

$$\lim_{P_P(k)\to 0} G_P(k) = 1 \quad \lim_{P_P(k)\to P_{P,total}^{max}} G_P(k) = \frac{1}{1+g_1}$$

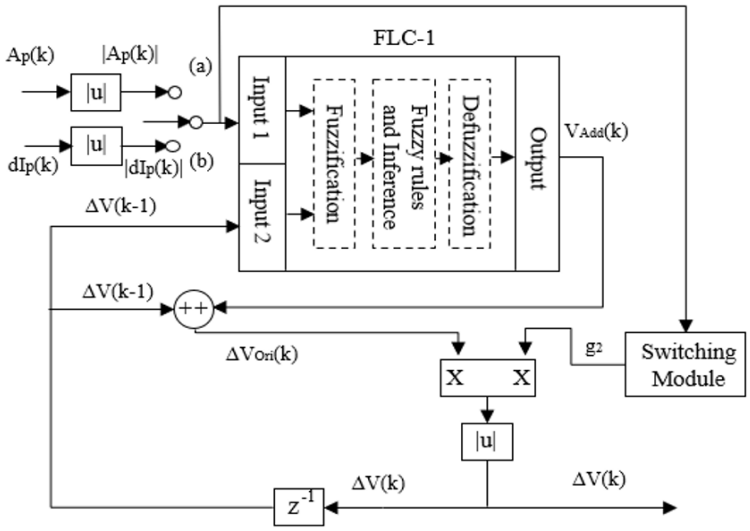

Figure 5. PV panel's power-voltage (P-V) curve.

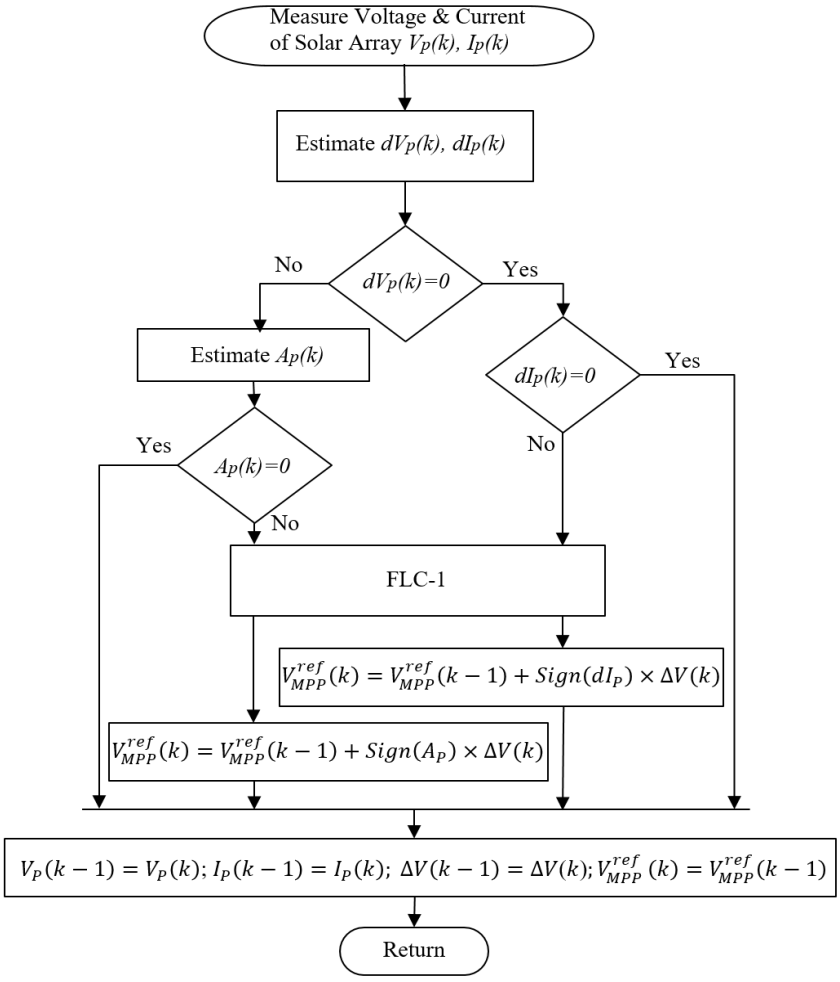

Figure 6. INC-MPPT algorithm with Fuzzy logic.

$$P_P(k) = V_P(k) \times I_P(k) \tag{4}$$

Preprints (www.preprints.org) | NOT PEER-REVIEWED | Posted: 3 December 2021 doi:10.20944/preprints202112.0044.v1

$$dI_P(k) = I_P(k) - I_P(k-1) \quad (5)$$

$$dV_P(k) = V_P(k) - V_P(k-1) \quad (6)$$

To avoid significant changes in the step-size and instability of the PV output power, a switching module is implemented as described in Figure 5. According to the first input, namely, $|A_P(k)|$ or $|dI_P(k)|$, the system will put appropriate output coefficient g_2 as shown in Table 3.

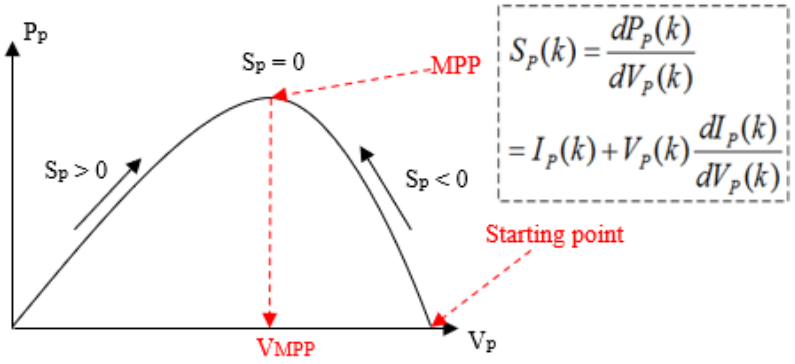

Figure 7. FLC-1 structure

Table 3. Switching Module Operation

(a): If the input is $\|A_P(k)\|$		(b): If the input is $\|dI_P(k)\|$
$\|A_P(k)\|>0.1$	$\|A_P(k)\|\leq 0.1$	$g_2 = 1$ (where every value of $\|dI_P(k)\|$)
$g_2 = 0.25$	$g_2 = 0.1$	

As it is known from previous parts of the paper, the inputs are in a range of [0, 1]. It should be noted that all the inputs have the same number of linguistic variables, specifically five linguistic variables: VS – Very Small, SM – Small, ME – Medium, LA – Large, VL – Very Large. The output has nine linguistic variables, and they are in a range of [-1, 1]; in detail, NL – Negative Large, NM – Negative Medium, NS – Negative Small, NZ – Negative Zero, ZE – Zero, PZ – Positive Zero, PS – Positive Small, PM – Positive Medium, PL – Positive Large. As a result, there are 49 fuzzy rules associated in the FLC-1.

All the association rules of the FLC-1 are shown in Table IV, where the membership functions of the inputs and output can be referred in [18]. To explain the fuzzy rules in Table IV, we can analyze several sample cases as follows. In the first case when the two inputs $\Delta V(k-1)$ and $|dI_P(k)|$ are VS, that means the PV system is close to the MPP and the step voltage is also very small; thus, the output of the FLC-1 as the additional voltage $V_{add}(k)$ should be ZE to avoid fluctuations in the PV voltage at the steady state. Whereas, in another case is when $\Delta V(k-1)$ is LA and $|dI_P(k)|$ is ME, the additional voltage $V_{add}(k)$ will be NZ because the tendency of the PV system is on the way of automatically approaching the MPP. On the other hand, when the $\Delta V(k-1)$ is VS and $|dI_P(k)|$ is VL, that means the PV system is far away the MPP; therefore, the output $\Delta V(k-1)$ should be PL to force the PV system to quickly move to the MPP. In general, the other fuzzy rules in Table 4 can be suitably interpreted with the same deductive method.

Table 4. Fuzzy Rules for FLC-1

Preprints (www.preprints.org) | NOT PEER-REVIEWED | Posted: 3 December 2021 doi:10.20944/preprints202112.0044.v1

$V_{add}(k)$		$\lvert A_P(k)\rvert$ or $\lvert dI_P(k)\rvert$				
		VS	SM	ME	LA	VL
$\Delta V(k-1)$	VS	ZE	PZ	PS	PM	PL
	SM	NZ	ZE	PZ	PS	PM
	ME	NS	NZ	ZE	PZ	PS
	LA	NM	NS	NZ	ZE	PZ
	VL	NL	NM	NS	NZ	ZE

3.1.2. PI controller

The PI controller with anti-windup block (referred in [21]) serves as the second sub-controller of the system. Figures 4 and 8 demonstrate detailed schematics of the controller.

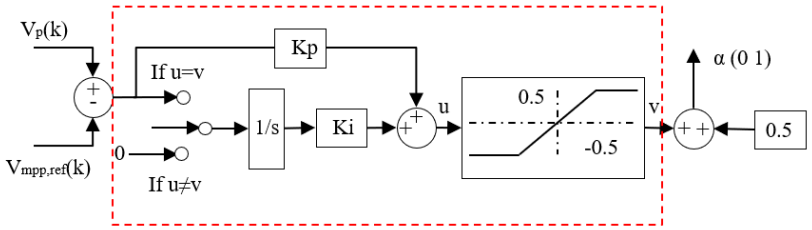

Figure 8. PI-1 controller in detail

3.2. DC Link Voltage Regulator Module

According to Figure 3, the DC-link voltage regulator should find an optimal value of reference current to make V_{DC} reach V_{DC}^{ref} [7, 8]. The output power which is supplied to the grid P_{AC} and the power of PV panel P_P have the following relation:

$$P_{AC} = (\eta_{DC-AC} \times \eta_{DC-DC})P_P = \eta_{Exp}P_P \quad (7)$$

where:
$\eta_{DC\text{-}DC}$ – efficiency of the buck-boost DC-DC converter
$\eta_{DC\text{-}AC}$ – efficiency of the DC-AC inverter
$\eta_{DC}=\eta_{DC\text{-}DC}\,\eta_{DC\text{-}AC}$ – overall efficiency of PV system
Equation (7) can be written as:

$$V_g I_g(\cos\theta_g) = \eta_{Exp}P_P \quad (8)$$

where $\cos\theta_g$ is the power factor of the PV system, V_g is the rms value of the grid voltage, and I_g is the rms value of the grid current. In the normal operation of the grid, the rms value of the grid voltage is often larger than zero, it means $V_g > 0$ V.
Hence,

$$I_g = \eta_{Exp}\frac{P_P}{V_g(\cos\theta_g)} \quad (9)$$

When the PF = 1, the grid current will reach the desired value.

$$I_g^{ref} = \eta_{Exp}\frac{P_P}{V_g} \quad (10)$$

But overall efficiency depends not only on the PF, but also on other components parameters and too complicated to estimate. This issue can be solved by implementing fuzzy

Preprints (www.preprints.org) | NOT PEER-REVIEWED | Posted: 3 December 2021 doi:10.20944/preprints202112.0044.v1

logic controller to update frequently η_{Exp} (Refer to Figure 9). The FLC-2 is aimed to improve the PI controller. It has two inputs and one output.

The two inputs:

$e_{Vdc}(k)$ – error between desired and present DC link voltage

$de_{Vdc}(k)$ – change in error

The output:

$\Delta\eta(k)$ – step in efficiency, added to the overall efficiency η_{Exp} to reach the desired value:

$$\eta_{Exp}(k) = \eta_{Exp}(k-1) + \Delta\eta(k) \tag{11}$$

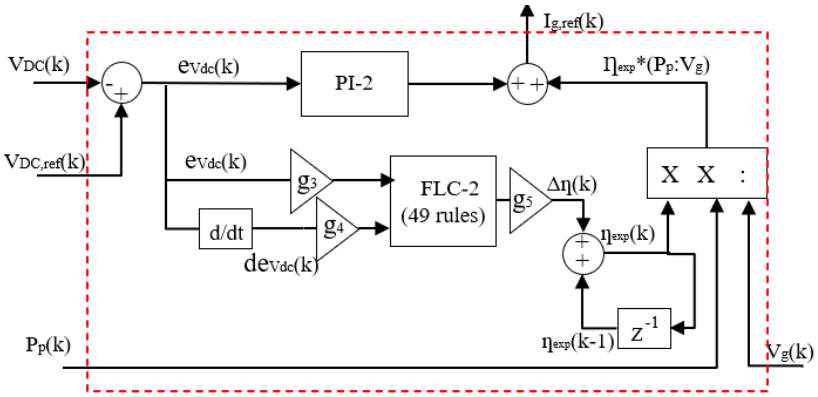

Figure 9. PI-Fuzzy hybrid controller schematic where g_3, g_4 and g_5 are design coefficients

The two inputs:

$$e_{Vdc}(k) = V_{DC}^{ref} - V_{DC}(k) \tag{12}$$

$$de_{Vdc}(k) = e_{Vdc}(k) - e_{Vdc}(k-1) \tag{13}$$

All the inputs have the same number of linguistic variables, specifically 7, the range is [-20, 20]: NL – Negative Large, NM – Negative Medium, NS – Negative Small, ZE – Zero, PS – Positive Small, PM – Positive Medium, PL – Positive Large

The output ($\Delta\eta(k)$) has nine linguistic variables, and they range from [-1 1]: NL – Negative Large, NM – Negative Medium, NS – Negative Small, NZ – Negative Zero, ZE – Zero, PZ – Positive Zero, PS – Positive Small, PM – Positive Medium, PL – Positive Large. As a result, there are 49 fuzzy rules formed in the FLC-2.

All the association rules of the FLC-2 are presented in Table 5, where the membership functions of the inputs and output can be referred in [18]. To interpret the fuzzy rules in Table V, we can analyze and evaluate some sample cases as follows. Firstly, when $de_{Vdc}(k)$ is NL and $e_{Vdc}(k)$ is PL, the output of this fuzzy controller $\Delta\eta(k)$ should be ZE since the tendency of the DC-link voltage $V_{dc}(k)$ is on the way of automatically approaching its reference value. On the other hand, when $de_{Vdc}(k)$ is ZE and $e_{Vdc}(k)$ is NL, that means $V_{dc}(k)$ is much smaller than its reference value; thus, the output $\Delta\eta(k)$ should be PL to force Vdc(k) to rapidly move to its desired value. Besides, when $de_{Vdc}(k)$ is ZE and $e_{Vdc}(k)$ is PS, that means Vdc(k) is marginally larger than its reference value; hence, the output $\Delta\eta(k)$ should be NS to slightly decrease $V_{dc}(k)$ to its desired value without the oscillation at the steady state. In general, the other fuzzy rules in Table 5 can be appropriately explained with the similar deductive technique.

Table 5. Fuzzy Rules for FLC-2

$\Delta\eta(k)$	$e_{Vdc}(k)$						
	NL	NM	NS	ZE	PS	PM	PL
NL	PU	PU	PL	PL	PM	PS	ZE

Preprints (www.preprints.org) | NOT PEER-REVIEWED | Posted: 3 December 2021 doi:10.20944/preprints202112.0044.v1

$de_{Vdc}(k)$	NM	PU	PL	PL	PM	PS	ZE	NS
	NS	PL	PL	PM	PS	ZE	NS	NM
	ZE	PL	PM	PS	ZE	NS	NM	NL
	PS	PM	PS	ZE	NS	NM	NL	NL
	PM	PS	ZE	NS	NM	NL	NL	NU
	PL	ZE	NS	NM	NL	NL	NU	NU

3.3. Current Controller Module

In this section, the current controller is designed by an optimal control method. Firstly, from (2), we have the following dynamic model,

$$\begin{cases} \dot{x}_4 = -\frac{R}{L}x_4 - \frac{1}{L}x_5 + \frac{u}{L} \\ \dot{x}_5 = \frac{1}{C}x_4 - \frac{1}{C}x_6 \\ \dot{x}_6 = \frac{1}{L_g}x_5 - \frac{R_g}{L_g}x_6 - \frac{1}{Lg}V_g \end{cases} \tag{14}$$

The main purpose of the current controller is to keep the grid current ig (i.e., x_6) converge to its reference x6ref. Then, from the third equation of (14), the error dynamics of x_6 and the reference for x_5 (i.e., x_{5ref}) can be derived as,

$$\dot{x}_6 - \dot{x}_{6ref} = \frac{1}{L_g}\left((x_5 - x_{5ref}) + x_{5ref}\right) - \frac{R_g}{L_g}\left((x_6 - x_{6ref}) + x_{6ref}\right) - \frac{1}{L_g}V_g \tag{15}$$

So we have,

$$\dot{\tilde{x}}_6 = \frac{1}{L_g}\tilde{x}_5 - \frac{R_g}{L_g}\tilde{x}_6 - \frac{1}{L_g}x_{5ref} \tag{16}$$

where x_{5ref} is determined by

$$x_{5ref} = R_g x_{6ref} + v_g + \dot{x}_{6ref}L_g \tag{17}$$

Similarly, with x_{5ref} achieved from (17), combine with the second equation of (14),

$$\dot{x}_5 - \dot{x}_{5ref} = \frac{1}{C}\left((x_4 - x_{4ref}) + x_{4ref}\right) - \frac{1}{C}\left((x_6 - x_{6ref}) + x_{6ref}\right) \tag{18}$$

then

$$\dot{\tilde{x}}_5 = \frac{1}{C}\tilde{x}_4 - \frac{1}{C}\tilde{x}_6 \tag{19}$$

where

$$x_{4ref} = x_{6ref} + \dot{x}_{5ref}C_f \tag{20}$$

From x_{5ref} and x_{4ref} obtained in (17) and (20), respectively, the first equation of (14) can be rewritten as

$$\dot{\tilde{x}}_4 = -\frac{R}{L}\tilde{x}_4 - \frac{R}{L}x_{4ref} - \frac{1}{L}\tilde{x}_5 - \frac{1}{L}x_{5ref} - \dot{x}_{4ref} + \frac{1}{L}u_1 + \frac{1}{L}u_2 \tag{21}$$

Hence, we have

$$\dot{x}_4 = -\frac{R}{L}\tilde{x}_4 - \frac{1}{L}\tilde{x}_5 + \frac{1}{L}u_1 \tag{22}$$

where

$$u_2 = Rx_{4ref} + x_{5ref} + L\dot{x}_{4ref} \tag{23}$$

Preprints (www.preprints.org) | NOT PEER-REVIEWED | Posted: 3 December 2021 doi:10.20944/preprints202112.0044.v1

Here, we decompose the control input u into two terms: u_1 and u_2; in detail, u_1 is used for feedback control to stabilize the error dynamics, whereas u_2 is the compensating term used to compensate for the offset in the reference tracking problem. Finally, the error dynamics of (15) is achieved by combining (22), (19) and (16), as follows,

$$\begin{bmatrix} x_4 \\ x_5 \\ x_6 \end{bmatrix} = \begin{bmatrix} -\frac{R_g}{L_g} & \frac{1}{L_g} & 0 \\ -\frac{1}{L} & 0 & \frac{1}{C} \\ 0 & -\frac{1}{L} & -\frac{R}{L} \end{bmatrix} + \begin{bmatrix} 0 \\ 0 \\ \frac{1}{L} \end{bmatrix} u_1 \tag{24}$$

Equation (24) is rewritten in the following form,

$$\dot{x} = Ax + Bu_1 \tag{25}$$

Consider the following cost function,

$$J(x,u) = \int_0^\infty x^T Q x + u_1^T Q u_1 \tag{26}$$

where $Q \geq 0$ and $R > 0$ are the weighting matrices with appropriate dimensions, that is 3x3 and a scalar, respectively. After that, this cost function is minimized by the following control law:

$$u_1 = -Kx = -R^{-1}B^T P x \tag{27}$$

where K is the controller gain matrix, and P is the positive definite solution of the algebraic Riccati equation as follows

$$PA + A^T P - PBR^{-1}B^T P + Q = 0 \tag{28}$$

Typically, Q is chosen to be diagonal:

$$Q = \begin{bmatrix} q_1 & 0 & 0 \\ 0 & q_2 & 0 \\ 0 & 0 & q_3 \end{bmatrix} \tag{29}$$

where its elements and R can be selected by the following criteria,

$$q_i = \frac{1}{t_{si}(x_{imax})^2}, R = \frac{1}{(u_{1max})^2}, p > 0 \tag{30}$$

In (30), x_{imax} is $|x_i|$ constraint, u_{imax} is $|u_i|$ constraint, and t_{si} is the required settling time of x_i.

4. Simulation Results

The simulation performed in MATLAB/Simulink and all related parameters of the considered PV system can be referred in [18]. The results with the designed LQR control are illustrated in Figures 10-13, in which the time unit in the horizontal axis is second.

4.1. Simulation 1: Constant air temperature

This case considers when temperature is constant and 25°C. Irradiation starts from 850 W/m² at a time from 0 s to 0.3 s, then it becomes 1000 W/m² from 0.3 s to 0.6 s and finally becomes 400 W/m² from 0.6 s to 0.9 s. Figure 17 shows that results of the VP is close to the reference value. The obtained output powers of the PV array are 847 W, 998 W and 385 W which matches to the reference data provided in Table 1. Thus, this means that the power loss is small in this test.

Besides, the DC-link voltages correspond to each other in Figure 13. Furthermore, the grid current is equal to reference values. Finally, it was shown and proved that the voltage and

Preprints (www.preprints.org) | NOT PEER-REVIEWED | Posted: 3 December 2021 doi:10.20944/preprints202112.0044.v1

current of the grid are in phase, that means the power factor of the grid-connected PV system is nearly unity.

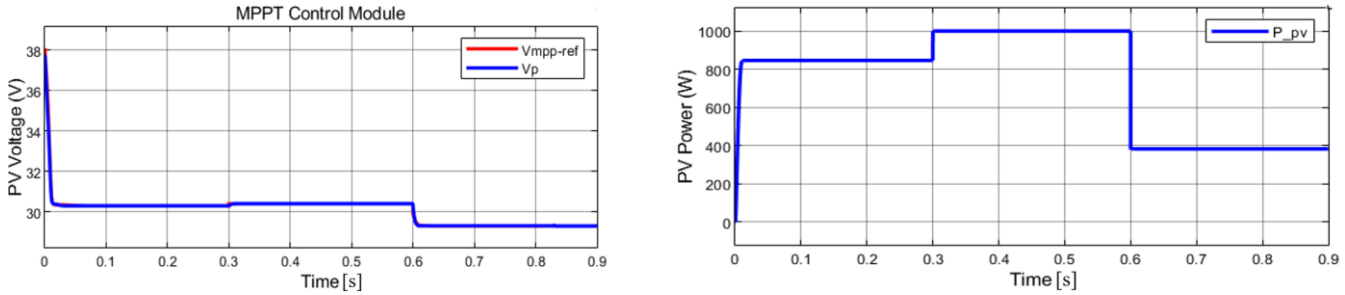

(**a**) (**b**)

Figure 10. MPPT module performance. (a) PV voltage; (b) PV output power

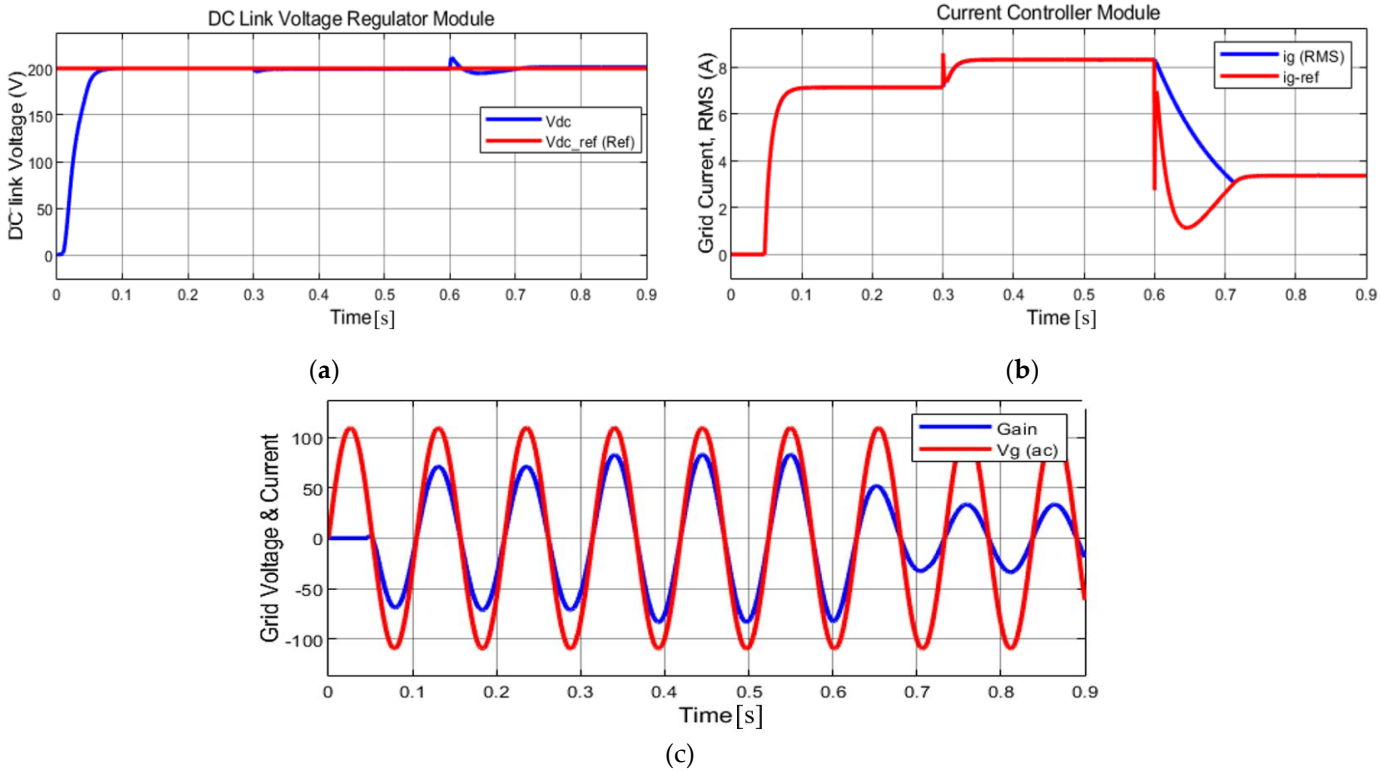

(**a**) (**b**)

(c)

Figure 11. DC Link Voltage Regulator module and Current Controller module performances with LQR method. (a) DC-link voltage; (b) Grid current's magnitude; (c) Grid voltage waveform V_g(V) and current waveform where Gain is 10 x I_g (A)

4.2. Simulation 2: Constant solar irradiation

In the second case solar irradiation is constant, 1000 W/m², but temperature is varying. From t = 0 s to 0.3 s temperature is 25℃, next 0.3 s temperature is 45℃, and last 0.3 s temperature level is 30℃. According to Figure 14 performance of the panel: 30.38 V / 1000 W, 27.92 V / 912.1 W and 29.76 V / 978.8 W which highly close to the values represented in Table 1. Despite the temperature change V_{DC} all the time was matching its reference. In addition, the RMS value of I_g is maintained according to the reference trend. The phases of the grid voltage and current match together, which means that the system's power factor is unity.

Preprints (www.preprints.org) | NOT PEER-REVIEWED | Posted: 3 December 2021 doi:10.20944/preprints202112.0044.v1

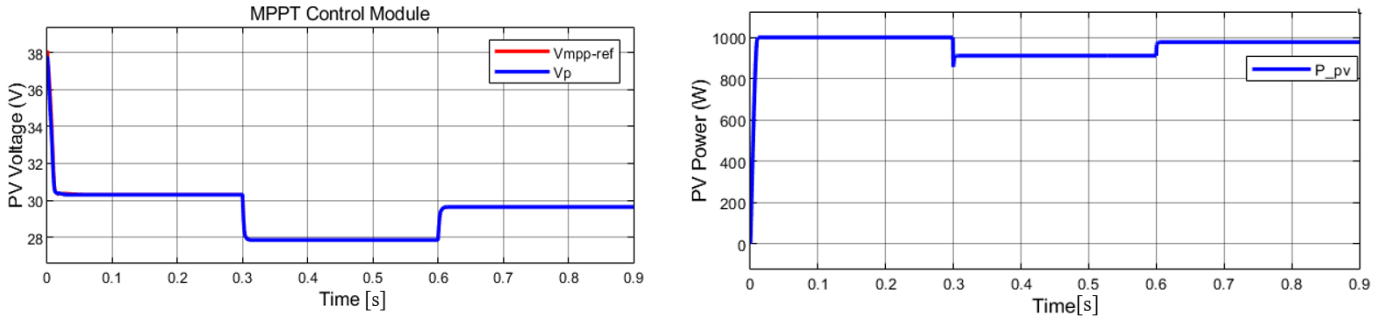

(a) (b)

Figure 12. MPPT module performance. (a) PV voltage; (b) PV output power

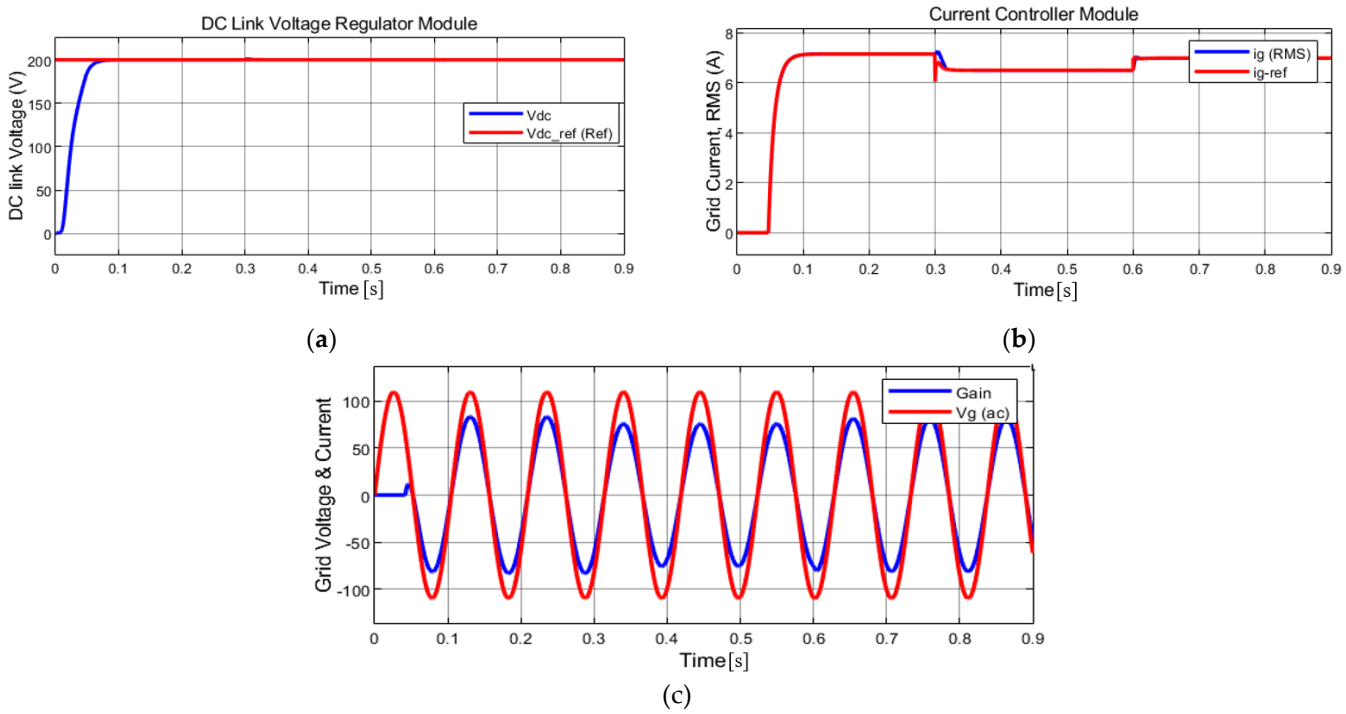

(a) (b)

(c)

Figure 13. DC Link Voltage Regulator module and Current Controller module performances with LQR method. (a) DC-link voltage; (b) Grid current's magnitude; (c) Grid voltage waveform V_g (V) and current waveform where Gain is 10 x I_g (A)

5. Comparison Between LQR and Backstepping Approaches

This research suggests the suitable combination of LQR and fuzzy control for the grid-connected PV systems. To show the effectiveness of the provided technique, it is important to make comparison between some other method, such as photovoltaic grid-connected system using fuzzy logic and backstepping approach [18] (see this reference paper to get the specific details of simulations). Figures 14-17 present the simulation results of fuzzy control and backstepping approach for the grid-connected photovoltaic system with the constant air temperature (Figures 10 and 11) and with the constant solar irradiation (Figures 14 and 15), in which the time unit in the horizontal axis is second. The obtained simulation results should be compared to results of abovementioned method. Specifically, the results with Figures 12 and 13 should be contrasted with that with Figures 16 and 17. We can see that both the control methods have shown good results.

It is obvious that simulation results of MPPT parts in both the cases are same since the main changes were not related to MPPT, but LQR. Thus, the behaviors shown in Figures 12 and 16 are same; the performances presented in Figures 12 and 16 are also similar. Comparing the DC-link Voltage Regulator Module and Current Controller Module of both the cases, it is clearly seen that LQR case reacts to the changes in temperature and

Preprints (www.preprints.org) | NOT PEER-REVIEWED | Posted: 3 December 2021 doi:10.20944/preprints202112.0044.v1

irradiation faster, in other words, the settling time of the LQR technique is lower compared to backstepping method. Moreover, LQR method is robust to different temperature and irradiation changes, which makes this technique preferable. In addition, in the case of backstepping method overshooting of the signal was observed, which significantly degrades the output and overall efficiency of the considered PV system. Furthermore, the response speed of the designed LQR is faster, consequently the rise time and peak time of the LQR are lower than that of backstepping approach.

5.1. Simulation 1: Constant air temperature

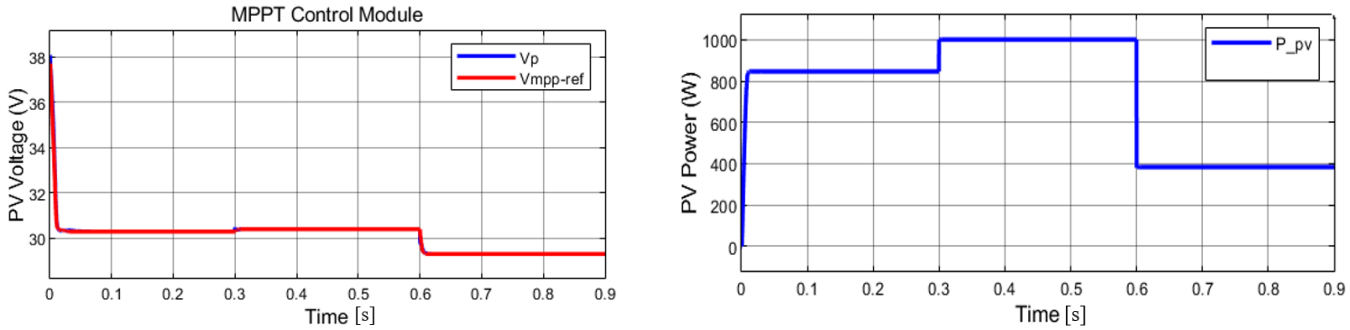

(**a**) (**b**)

Figure 14. MPPT module performance in case with backstepping approach. (a) PV voltage; (b) PV output power

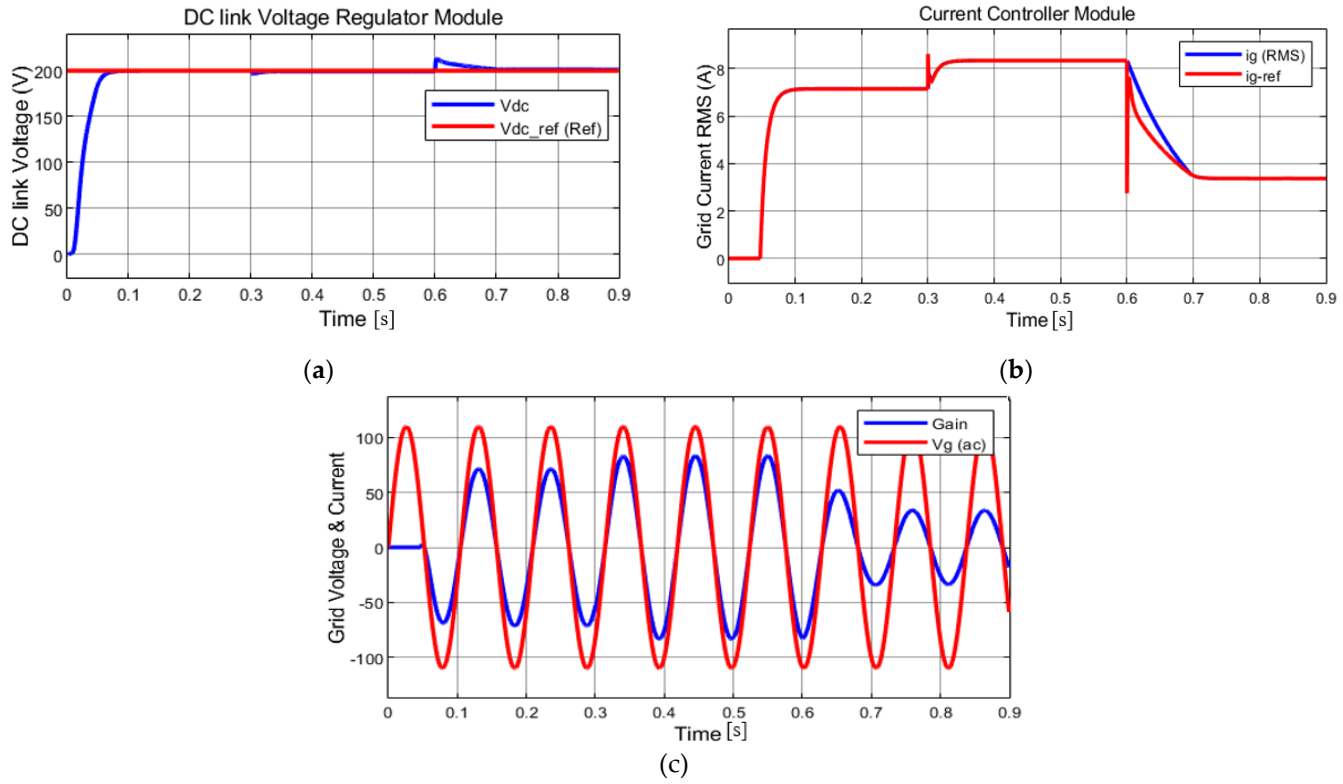

(**a**) (**b**)

(c)

Figure 15. DC Link Voltage Regulator module and Current Controller module performances with backstepping approach. (a) DC-link voltage; (b) Grid current's magnitude; (c) Grid voltage waveform V_g (V) and current waveform where Gain is 10 x I_g (A)

5.2. Simulation 2: Constant solar irradiation

Preprints (www.preprints.org) | NOT PEER-REVIEWED | Posted: 3 December 2021 doi:10.20944/preprints202112.0044.v1

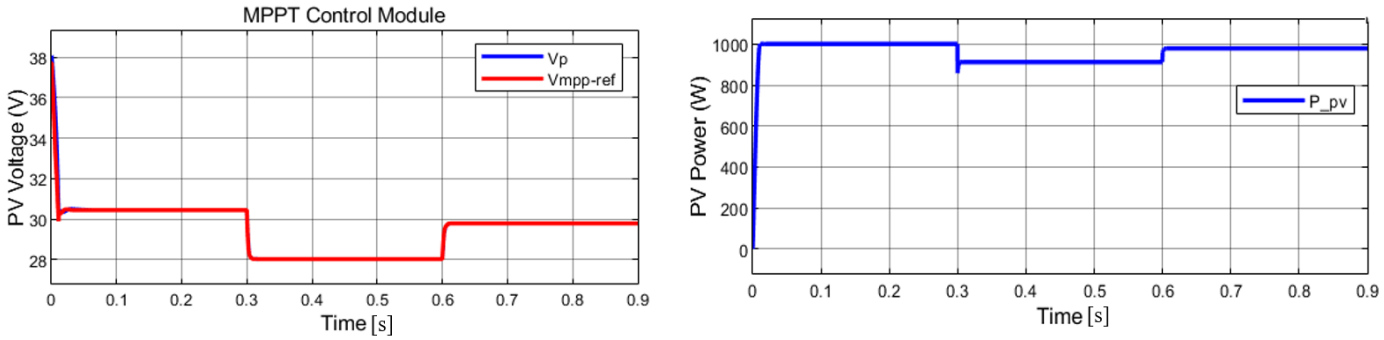

(**a**) (**b**)

Figure 16. MPPT module performance in case with backstepping approach. (a) PV voltage; (b) PV output power

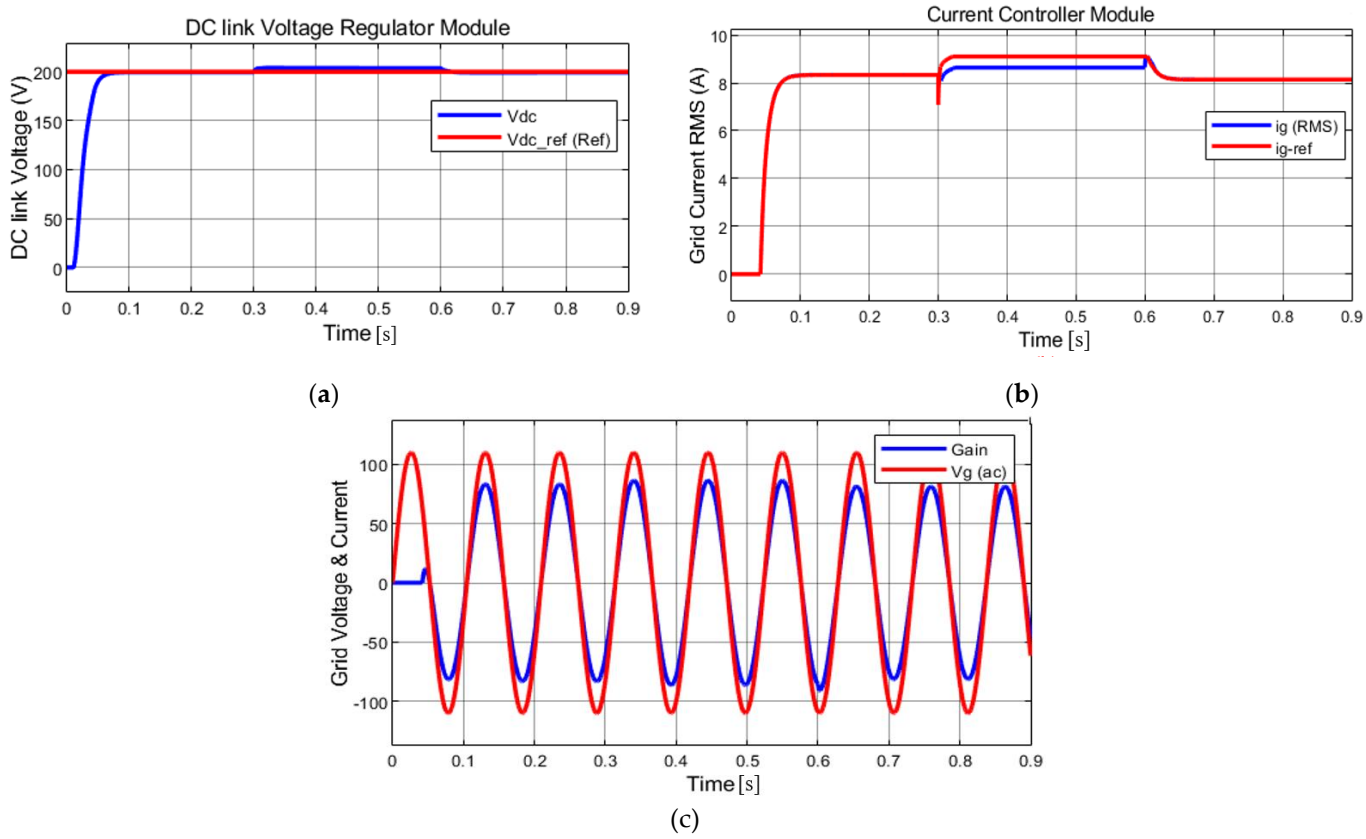

(**a**) (**b**)

(c)

Figure 17. DC Link Voltage Regulator module and Current Controller module performances with backstepping approach. (a) DC-link voltage; (b) Grid current's magnitude; (c) Grid voltage waveform V_g (V) and current waveform where Gain is 10 x I_g (A)

6. Conclusions

Based on fuzzy control and LQR, this study provided a comprehensive control solution for the grid-connected single-phase PV systems. In terms of improving the quality of controller methods, this work represented a substantial extension and enhancement of our past research in [18]. For the grid-connected solar systems, the suggested approach is the LQR suitably combined with fuzzy control, in which the design procedures of all the controllers are also described in detail. The major novelty of this study was to demonstrate and verify that the newly proposed approach is more successful in different aspects by comparing our past and present control methods. The LQR technique's major benefit is its ability to react quickly to unexpected changes in the system, such as changes in the air temperature and solar irradiation. In other words, the systems achieve their settling period sooner, which is necessary to steady the output behavior.

Furthermore, as compared to backstepping approach, the LQR method is more resistant to various changes in the weather condition. The backstepping approach also has the greater overrun, which has a detrimental influence on the efficiency of the investigated PV system. As previously stated, the LQR has the quicker response speed, making this type of controller more desirable. These are the major contributions of our present work as compared to the earlier research in [18]. Moreover, the results of simulations under different weather circumstances were compared to theoretical ones to indicate that the proposed system can cope with variations in weather parameters well. It was also demonstrated that abrupt changes in weather factors had no significant effects on the proposed control system's performance.

In future work, intelligent models based on fuzzy control for effectively predicting the PV power and load demand [22] will be thoroughly studied and implemented to improve the effectiveness and quality of the grid-connected solar energy systems.

Author Contributions: A.M. worked on all the tasks, T.D and N.T. worked on model and control designs and performed supervision. All authors participated in writing and review. All authors have read and agreed to the published version of the manuscript.

Funding: This work was supported by Nazarbayev University under the Faculty Development Competitive Research Grant Program (FDCRGP), Grant No. 11022021FD2924.

Conflicts of Interest: The authors declare no conflict of interest.

References

1. Torquato, R.; Arguello, A.; Freitas, W. Practical Chart for Harmonic Resonance Assessment of DFIG-Based Wind Parks. IEEE Trans. Power Deliv. 2020, 35, 2233–2242, doi:10.1109/TPWRD.2020.2964631.
2. Thao, N.G.M.; Uchida, K.; Kofuji, K.; Jintsugawa, T.; Nakazawa, C. A comprehensive analysis study about harmonic resonances in megawatt grid-connected wind farms. 3rd Int. Conf. Renew. Energy Res. Appl. ICRERA 2014 2014, 387–394, doi:10.1109/ICRERA.2014.7016415.
3. Alajmi, B.N.; Ahmed, K.H.; Finney, S.J.; Williams, B.W. Fuzzy-logic-control approach of a modified hill-climbing method for maximum power point in microgrid standalone photovoltaic system. IEEE Trans. Power Electron. 2011, 26, 1022–1030, doi:10.1109/TPEL.2010.2090903.
4. Kottas, T.L.; Boutalis, Y.S.; Karlis, A.D. New maximum power point tracker for PV arrays using fuzzy controller in close cooperation with fuzzy cognitive networks. IEEE Trans. Energy Convers. 2006, 21, 793–803, doi:10.1109/TEC.2006.875430.
5. Hamidia, F.; Abbadi, A.; Boucherit, M.S. Maximum Power Point Tracking Control of Photovoltaic Generation Based on Fuzzy Logic. Lect. Notes Networks Syst. 2018, 35, 197–205, doi:10.1007/978-3-319-73192-6_20.
6. Menniti, D.; Pinnarelli, A.; Brusco, G. Implementation of a novel fuzzy-logic based MPPT for grid-connected photovoltaic generation system. 2011 IEEE PES Trondheim PowerTech Power Technol. a Sustain. Soc. POWERTECH 2011 2011, doi:10.1109/PTC.2011.6019369.
7. Yang, B.; Li, W.; Zhao, Y.; He, X. Design and analysis of a grid-connected photovoltaic power system. IEEE Trans. Power Electron. 2010, 25, 992–1000, doi:10.1109/TPEL.2009.2036432.
8. Fadil, H. El; Giri, F.; Guerrero, J.M. Grid-connected of photovoltaic module using nonlinear control. Proc. - 2012 3rd IEEE Int. Symp. Power Electron. Distrib. Gener. Syst. PEDG 2012 2012, 119–124, doi:10.1109/PEDG.2012.6253989.
9. Wai, R.J.; Wang, W.H. Grid-connected photovoltaic generation system. IEEE Trans. Circuits Syst. I Regul. Pap. 2008, 55, 953–964, doi:10.1109/TCSI.2008.919744.
10. Reddy, D.; Ramasamy, S. A fuzzy logic MPPT controller based three phase grid-tied solar PV system with improved CPI voltage. 2017 Innov. Power Adv. Comput. Technol. i-PACT 2017 2017, 2017-Janua, 1–6, doi:10.1109/IPACT.2017.8244953.
11. Kumar, J.; Rathor, B.; Bahrani, P. Fuzzy and P amp; O MPPT techniques for stabilized the efficiency of solar PV system. 2018 Int. Conf. Comput. Power Commun. Technol. GUCON 2018 2019, 259–264, doi:10.1109/GUCON.2018.8674909.
12. Andrew-Cotter, J.; Nasir Uddin, M.; Amin, I.K. Particle swarm optimization based adaptive neuro-fuzzy inference system for MPPT control of a three-phase grid-connected photovoltaic system. 2019 IEEE Int. Electr. Mach. Drives Conf. IEMDC 2019 2019, 2089–2094, doi:10.1109/IEMDC.2019.8785403.
13. Arulkumar, K.; Palanisamy, K.; Vijayakumar, D. Recent advances and control techniques in grid connected Pv system - A review. Int. J. Renew. Energy Res. 2016, 6, 1037–1049.
14. Blaabjerg, F.; Teodorescu, R.; Liserre, M.; Timbus, A. V. Overview of control and grid synchronization for distributed power generation systems. IEEE Trans. Ind. Electron. 2006, 53, 1398–1409, doi:10.1109/TIE.2006.881997.
15. R. Teodorescu, F. Blaabjerg, M.L. and P.C.L. Proportional-resonant controllers and filters for grid-connected voltage-source converters. IEE Proceedings-Electric Power Appl. 2006, 153, doi:10.1049/ip-epa:20060008.

16. Wu, R., Dewan, S. B. and Slemon, G.R. Analysis of a PWM AC to DC Voltage Source Converter under the Predicted Current Control with a Fixed Switching Frequency. IEEE Trans. Ind. Appl. 1991, 27, 756–764.
17. Zhang, K.; Kang, Y.; Xiong, J.; Chen, J. Direct repetitive control of SPWM inverter for UPS purpose. IEEE Trans. Power Electron. 2003, 18, 784–792, doi:10.1109/TPEL.2003.810846.
18. Thao, N.G.M.; Uchida, K. Control the photovoltaic grid-connected system using fuzzy logic and backstepping approach. 2013 9th Asian Control Conf. ASCC 2013 2013, doi:10.1109/ASCC.2013.6606123.
19. Liserre, M.; Blaabjerg, F.; Hansen, S. Design and control of an LCL-filter-based three-phase active rectifier. IEEE Trans. Ind. Appl. 2005, 41, 1281–1291, doi:10.1109/TIA.2005.853373.
20. Sun, W.; Chen, Z.; Wu, X. Intelligent optimize design of LCL filter for three-phase voltage-source PWM rectifier. 2009 IEEE 6th Int. Power Electron. Motion Control Conf. IPEMC '09 2009, 3, 970–974, doi:10.1109/IPEMC.2009.5157524.
21. Li, X.L.; Park, J.G.; Shin, H.B. Comparison and evaluation of anti-windup PI controllers. J. Power Electron. 2011, 11, 45–50, doi:10.6113/JPE.2011.11.1.045.